HPU2 Journal of Sciences:
Natural Sciences and Technology

Journal homepage: https://sj.hpu2.edu.vn

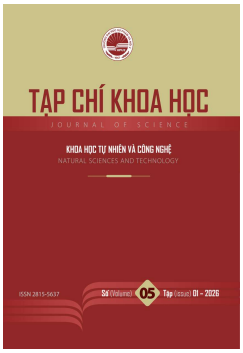

Article type: Research article

Non-uniform lagrange interpolation in B-mode ultrasound image reconstruction

The-Lam Nguyen*, Van-Duong Nguyen, Quang-Huy Tran

Hanoi Pedagogical University 2, Phu Tho, Vietnam

Abstract

This study introduces a signal-processing framework based on non-uniform Lagrange interpolation for improving spatial sampling consistency in ultrasound imaging. The proposed method adaptively adjusts pixel coordinates to make the effective sampling density across the reconstructed image more uniform, thereby mitigating the geometric distortion commonly observed in conventional B-mode ultrasound data. To experimentally validate the approach, a compact B-mode ultrasound acquisition system was developed using an Arduino-based transmitter–receiver module interfaced with a personal computer. The measured echo amplitudes reliably captured key acoustic characteristics of the examined medium, including transmission behavior, reflection properties, and attenuation effects. Following the acquisition, the signals were processed in MATLAB using the implemented non-uniform Lagrange interpolation algorithm. The results demonstrate that the method enables accurate and stable reconstruction of B-mode ultrasound images from the non-uniformly sampled echo data.

Keywords: Lagrange interpolation, ultrasound scanner, B-mode, ultrasound image, arduino

1. Introduction

Ultrasound imaging plays a central role in modern clinical diagnostics due to its safety, portability, and capability for real-time visualization of anatomical structures [1], [2]. In B-mode ultrasound, a sequence of A-mode echoes is acquired. At the same time, the transducer scans over a sector, producing image data that naturally follow a polar or block-arc acquisition geometry, rather than a Cartesian grid [3], [4]. Consequently, effective scan conversion and interpolation techniques are essential for transforming polar acoustic measurements into clinically meaningful Cartesian images [5], [6].

* Corresponding author, E-mail: nguyenthelam@hpu2.edu.vn

https://doi.org/10.56764/hpu2.jos.2025.5.1.27-34

Received date: 04-12-2025 ; Revised date: 11-3-2026 ; Accepted date: 30-3-2026

Conventional interpolation methods—including nearest-neighbor, bilinear, bicubic, and spline interpolation—are designed for uniformly sampled Cartesian data [7], [8]. When directly applied to ultrasound sector data, these methods often create non-uniform pixel distributions, leading to oversampled regions near the probe and undersampled regions at larger radii [9], [10]. Such inconsistencies degrade lateral resolution and introduce geometric distortions or artifacts that reduce the interpretability of reconstructed images [11]. While several scan-conversion strategies have been proposed for ultrasound, most employ fixed, uniform resampling patterns that do not account for the inherent radial variation in spatial sampling [12], [13].

In contrast, mathematical studies have shown that Lagrange polynomial interpolation provides a flexible and analytically robust framework for reconstructing functions from arbitrarily spaced sample points [14], [15]. Non-uniform interpolation techniques have also been successfully applied in areas such as image super-resolution and non-Cartesian MRI reconstruction, where sampling density varies spatially and uniform interpolation is inadequate [16]–[18]. These results suggest that explicitly modeling the non-uniform sampling geometry of ultrasound can yield more accurate scan-conversion and enhance the visual quality of B-mode images.

By sampling along concentric arcs (with constant radius) for each processing step, we effectively reduce the 2D interpolation problem to a series of 1D interpolation tasks. This allows adaptive pixel redistribution, where the number of interpolated pixels increases proportionally with the radius. Specifically, the pixel density can be doubled compared to the adjacent smaller arc, resulting in a non-uniform pixel distribution across different radius.

The development of low-cost ultrasound platforms has further enabled the practical evaluation of such algorithms. Recent open-hardware efforts demonstrate that single-element ultrasound imaging can be implemented using microcontroller-based systems and cost-effective analog front-ends [12], [19]. Commodity sensors such as the HC-SR04, though originally designed for distance measurements, have been adapted to extract analog echo amplitudes, providing a convenient platform for prototyping A-mode acquisition and testing scan-conversion algorithms [14], [15]. The combination of accessible hardware and powerful software tools such as MATLAB facilitates rapid development, real-time signal processing, and visualization of reconstructed images [20].

Motivated by the limitations of traditional uniform interpolation and the advantages of non-uniform sampling strategies, this study proposes a non-uniform Lagrange interpolation method tailored for B-mode ultrasound imaging. The proposed algorithm adaptively increases pixel density with radius, aligning with the natural sampling geometry of sector scans and resulting in a more uniform distribution of image information. We validate the method using experimental A-mode data acquired from a custom low-cost ultrasonic scanner, demonstrating improved continuity and detail in reconstructed B-mode images.

2. Non-uniform Lagrange interpolation

Conventional Lagrange interpolation is a powerful method for creating a polynomial that passes through a specific set of data points. The Lagrange interpolation method is very simple and intuitive for finding a polynomial function $P^n(x)$. It avoids solving a large system of linear equations to find the polynomial's coefficients. To clarify this issue, let's consider a set of $(n + 1)$ experimental data points.

x_0	x_1	x_2	…	…	x_{n-1}	x_n
y_0	y_1	y_2	…	…	y_{n-1}	y_n

The Lagrange basis polynomials at the i-th node $L_i(x)$ are defined as follows

$$L_i(x) = \prod_{k=0,k\neq i}^{n} \frac{(x-x_k)}{(x_i-x_k)} \quad (1)$$

Each Lagrange basis polynomial $L_i(x)$ has an important property

$$L_i(x_k) = \begin{cases} 1 & if\ k = i \\ 0 & if\ k \neq i \end{cases} \quad (2)$$

Thanks to this property, it is ensured that the interpolating polynomial $P^n(x)$ will pass through all the initial data points. Based on *n* reference points, the Lagrange interpolating polynomial has a maximum degree of *n* and is defined as follows:

$$P^n(x) = \sum_{i=0}^{n} y_i . L_i(x) \quad (3)$$

Assume that the initial result of an ultrasound image obtained from the scanner is in the form of a square matrix. In the polar coordinate system, the positions of the image pixels are determined as follows

$$x_{ij} = r_i . \cos(\varphi_j) \quad (4)$$

$$y_{ij} = r_i . \sin(\varphi_j) \quad (5)$$

where r_i is the radius of the i^{th} arc and φ_j is the scanning angle corresponding to the j^{th} pixel. For each arc, r_i is constant, so basically the coordinates of the pixels only depend on the scanning angle φ. Thus, we can write the coordinates of the image pixels as follows

$$r_{ij} = \sqrt{x_{ij}^2 + y_{ij}^2} \quad (6)$$

Or in the form of a square matrix *X* of order *n*

$$\mathrm{X} = \begin{pmatrix} r_{11} & r_{12} & \cdots & r_{1n} & r_{1(n+1)} \\ r_{21} & r_{22} & \cdots & r_{2n} & r_{2(n+1)} \\ & & & & \\ r_{n1} & r_{n2} & \cdots & r_{nn} & r_{(n+1)(n+1)} \end{pmatrix} \quad (7)$$

From the experimental data, the color of the pixels corresponding to the coordinates in (7) is normalized to the grayscale and is also written in the form of a matrix *Y* as

$$= \begin{pmatrix} c_{11} & c_{12} & \cdots & c_{1n} & c_{1(n+1)} \\ c_{21} & c_{22} & \cdots & c_{2n} & c_{2(n+1)} \\ & & & & \\ c_{n1} & c_{n2} & \cdots & c_{nn} & c_{(n+1)(n+1)} \end{pmatrix} \quad (8)$$

Using the i^{th} row data of both matrices *X* and *Y*, we can interpolate the i^{th} row of matrix *Y* with any number of elements. Define the interpolated variable as a vector $X^{(i)}$ with an arbitrary number of elements $(n + k)$.

$$X^{(i)} = (x_1^{(i)} \ \ x_2^{(i)} \ \ x_1^{(i)} \ \cdots \ x_{n+k-1}^{(i)} \ \ x_{n+k}^{(i)}) \quad (9)$$

where *k* is the number of added elements. To satisfy the interpolation condition, the first and last elements of vector $X^{(i)}$ are referenced against the i-th row of matrix *X* as $x_1^{(i)} = r_{i1}$ and $x_{n+1}^{(i)} = r_{i(n+1)}$. The interpolated elements of the i-th row of matrix *Y* are determined through the interpolation function.

$$Y^{(i)} = P^n(X^{(i)}) \quad (10)$$

3. Design and assembly of the simple ultrasonic scanner

Our ultrasonic scanner was designed according to the diagram in Figure 1. The ultrasonic frequency used is 40 (kHz). With this frequency, of course, we cannot scan internal body organs and tissues. Instead, we scan objects in air or water environments.

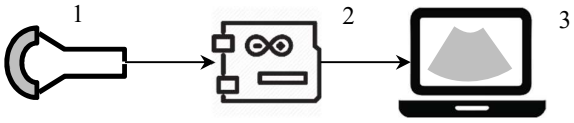

Figure 1. Block diagram of the ultrasonic scanner (1: Transducer, 2: Arduino, 3: PC).

The basic structure of the ultrasonic scanner includes the following components:

Transducer/Probe: This is the most important part of the ultrasonic machine, which transmits and receives ultrasonic waves. In this paper, we use the HC-SR04 ultrasonic sensor module. Since this module is designed for distance measurement, it cannot measure the amplitude of the reflected ultrasonic wave. To modify this module feature, based on the circuit diagram, we extracted a signal line from the receiver's output. After passing through a low-pass filter, the signal is fed directly into the Arduino's analog input (Figure 2).

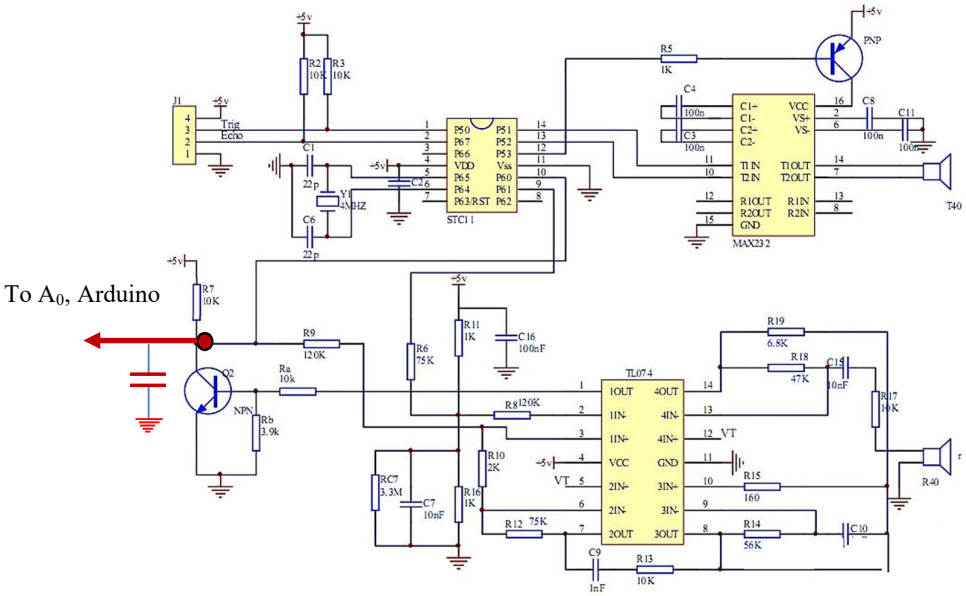

Figure 2. Circuit diagram of the HC-SR04 ultrasonic sensor module and the signal extraction point for the reflected wave amplitude.

Signal processor: The Arduino receives the reflected-sound-wave signals captured by the transducer as analog signals, $I(t)$. It converts these signals to digital values using the Arduino's ADC (analog-to-digital converter), then sends them to the computer via the USB port (Figure 3).

Figure 3. Arduino microcontroller and ADC conversion module.

Display: The computer receives the signals beam by beam and scans the entire space under investigation. Here, the computer calculates the attenuation coefficient at each pixel using a matlab program and then reconstructs the 2D image.

4. Experimentation and signal processing

The reflected ultrasonic wave amplitude signal over time, i(t), is acquired and sent to the Arduino's ADC converter and then transmitted to the computer's USB port via an embedded program written in C++. The experiment was conducted in an air environment with a speed of sound c = 343.2 (m/s). We can also convert the signal $I(t)$ (Figure 4) into a depth signal $I(r)$ (Figure 5). In the experiment, r is the radius of the pixel arc and can be calculated as follows:

$$x = \frac{c \times t}{2} \tag{11}$$

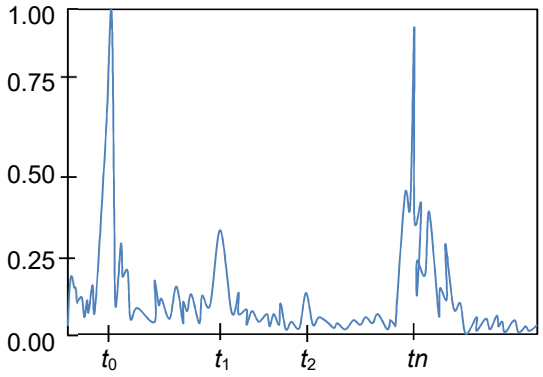

Figure 4. Reflected wave amplitude (dimensionless) received over time.

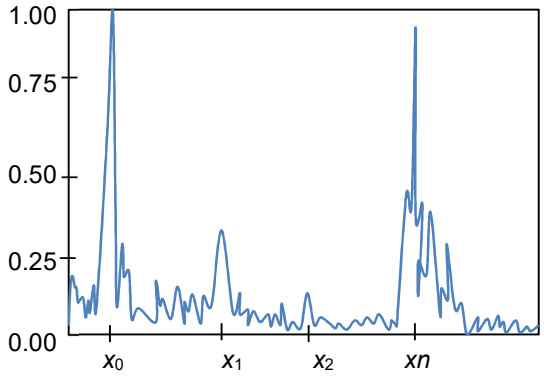

Figure 5. Reflected wave amplitude (dimensionless) received versus depth.

Because the amplitude of the sound wave attenuates with distance as $I(r) = I(0).\exp(-r)$, we amplified this signal with an approximate coefficient $K = r^2$, where r is the distance from the transducer to the reflecting surface. At a specific position of the transducer corresponding to the scanning angle φ, the reflected amplitude at the arc $r_{j+1} = r_j + dr$ (which is the position of the $(j + 1)^{th}$ point) on a scanned ray is recorded as follows:

$$I(x_{j+1}) = I(x_j).\exp(\alpha_j x_j) \sim I(x_i).\alpha_j x_j^2 \tag{12}$$

The attenuation coefficient of the medium calculated from the j^{th} arc to the $(j + 1)^{th}$ arc can be calculated as

$$\alpha_j = \frac{I(x_{j+1})}{x_i^2 . I(x_j)} \tag{13}$$

The attenuation coefficient α_j is proportional to the material density of the medium at the j^{th} point. To represent the alpha coefficients α_j using color, we use the grayscale color map in Matlab

$$Color_j = RGB(\alpha_j, \alpha_j, \alpha_j) \tag{14}$$

In our experiment, the scanning angle was performed at N = 81 positions from -40^0 to 40^0 with a step size of $d\varphi = 1^0$.

and at each scanning angle, the reflected signal is received at N = 81 arcs from 50 (mm) to 130 (mm) with a step size of $dr = 1$ (mm).

$$r_j = 50 + (j-1)dr \tag{15}$$

At each pixel position, the attenuation coefficients α_{ij} are converted equivalently to a grayscale variable according to (14) and (15). The matrix of pixels is then reconstructed in the form of a block arc, mirroring their natural positions during the scan (Figure 6).

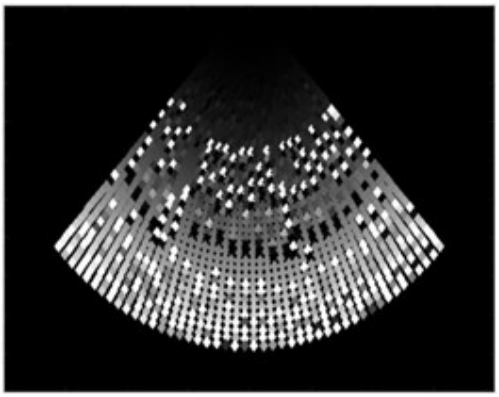

Figure 6. B-mode ultrasound image of the ultrasonic scanner with a size of 81×81pixels.

Figure 7. Initial ultrasound image with a size of 6×8 pixels.

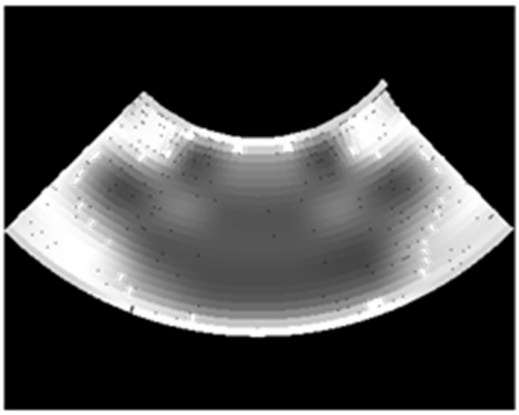

Figure 8. Ultrasound image after non-uniform interpolation with the number of pixels increasing with radius from 4.6×8.N.

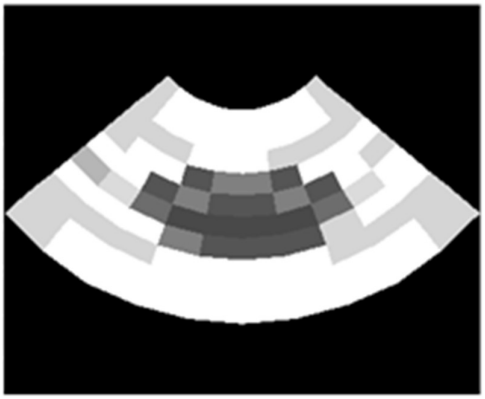

Figure 9. Initial ultrasound image with a size of 10×10 pixels.

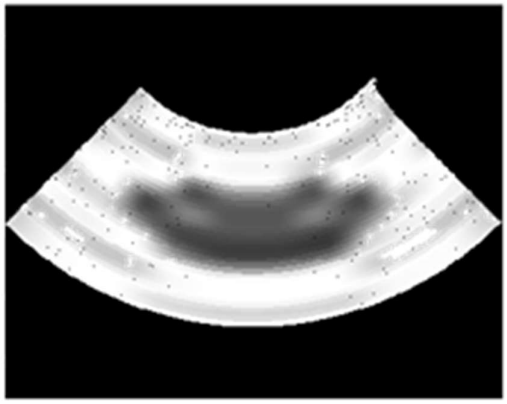

Figure 10. Ultrasound image after non-uniform interpolation with the number of pixels increasing with radius from 4.10×10.N.

To verify the non-uniform interpolation algorithm presented above, we experimentally scanned a foam object in the air, resulting in an image of size 4×8 pixels (Figure 7). After applying the non-uniform interpolation method, we obtained a higher quality ultrasound image (Figure 8). We have also included a comprehensive quantitative comparison using RMSE (Root-mean-square error), PSNR (Peak Signal-to-Noise Ratio) and SSIM (Structural Similarity Index), The results are presented in Table 1. These metrics provide a standardized measure of reconstruction fidelity and structural preservation..

Table 1. Quantitative metrics of RMSE, PSNR and SSIM.

Index	Value	Assessment
RMSE	12.45	The average error per pixel is moderate
PSNR	26.21 dB	The reconstruction quality is within an acceptable range for medical imaging (where a PSNR > 30 dB is typically considered good)
SSIM	0.784	Fair/Good

An SSIM value of 0.784 indicates that the method still exhibits internal structural discrepancies, influenced by high-frequency noise (visible as white speckles). Although the SSIM score is not yet at its peak, it reflects a successful transition from 'staircase artifacts' (resulting from discrete data) to a 'continuous representation', which is the primary objective of scan-conversion in medical imaging

5. Conclusions

In this paper, we addressed the following issues: we perfected the algorithm for non-uniform Lagrange interpolation for B-mode ultrasound image interpolation; we constructed a simple ultrasound machine using commercially available components. The ultrasound scanner operates well and stably in air and water environments. From this ultrasound machine, we acquired A-mode ultrasonic reflected wave signals; we successfully connected the reflected ultrasonic wave amplitude signal to a computer using the Arduino ADC converter with a connection program written in C+; the signal was processed and the B-mode ultrasound image was reconstructed by the computer with the support of Matlab software; the interpolated ultrasound image shows good quality and could potentially be used in medicine. Due to the too-low crystal frequency on the HC-SR04 module (40 kHz), imaging of the human body has not yet been

achieved. In this paper, we were also unable to filter the signal noise, so the initial image quality remains low. These issues will be addressed in subsequent work.

Lagrange interpolation with high-degree polynomials can lead to numerical instability, including arithmetic noise and spurious oscillations (Runge's Phenomenon). To overcome the numerical stability limitations of high-order polynomial interpolation, our future research will implement the Barycentric Lagrange formula or incorporate post-interpolation filtering, such as Median or Gaussian filter, to eliminate speckle noise. This approach not only ensures robust numerical stability but also optimizes computational speed for real-time execution.

References

[1] B. Luijten, M. van Sloun, A. de Jong, and T. van Walsum, "Ultrasound signal processing: From models to deep learning," Signal Processing, vol. 49, no. 3, pp. 677–698, Mar. 2023, doi: 10.1016/j.ultrasmedbio.2022.11.003.

[2] A. Abuhamad and R. Chaoui, First Trimester Ultrasound Diagnosis of Fetal Abnormalities, Lippincott Williams & Wilkins, 2018.

[3] C. Basoglu, "A real-time scan conversion algorithm on commercially available processors," Digital Signal Processing, vol. 6, no. 2, pp. 81–92, 1996.

[4] C. Fritsch and R. B. Thompson, "A multirate scan conversion method," Ultrasound, vol. 38, no. 1–8, pp. 179–182, Mar. 2000, doi: 10.1016/S0041-624X(99)00044-X.

[5] H. Liu, A. W. L. Fong, and R. T. Smith, "Image-interpolation methods for division-of-focal-plane polarimeters: a review," SPIE Proceedings, vol. 13189, 2024.

[6] Z. Chen, A. E. Carlton, and J. S. Tyo, "Calibration method of microgrid polarimeters with image interpolation," Applied Optics, vol. 54, no. 5, p. 995, Feb. 2015, doi: 10.1364/AO.54.000995.

[7] R. L. Burden and J. D. Faires, Numerical Analysis, 9th ed., Brooks/Cole, 2011. (Lagrange interpolation chapter).

[8] J. P. Berrut and L. N. Trefethen, "Barycentric Lagrange Interpolation," SIAM Review, vol. 46, no. 3, pp. 501–517, Jan. 2004, doi: 10.1137/S0036144502417715.

[9] A. Gilman and D. Bailey, "Near-optimal non-uniform interpolation for image super-resolution from multiple images," Proc. IVCNZ 2006, 2006.

[10] J. Schlemper, S. S. M. Salehi, P. Kundu, C. Lazarus, H. Dyvorne, D. Rueckert, and M. Sofka, "Nonuniform variational network: Deep learning for accelerated nonuniform MR image reconstruction," in Proc. MICCAI, 2019, pp. 57–64, doi: 10.1007/978-3-030-32248-9_7.

[11] K. L. Wright and J. P. Haldar, "Non-Cartesian parallel imaging reconstruction," NMR Biomed., 2014, doi: 10.1002/jmri.24521.

[12] L. Jonveaux, C. Hawkes, J. C. Valderrama, and L. Di Marco, "A low-cost, Arduino-like dev-kit for single-element ultrasound imaging," arXiv:1611.10174, 2016, doi: 10.5334/joh.2.

[13] L. Jonveaux et al., "Arduino-like development kit for single-element ultrasound imaging," Open Hardware, 2017, doi: 10.5334/joh.2.

[14] D. Abreu et al., "Low-cost ultrasonic range improvements for an assistive device", Sensors, 2021, doi: 10.3390/s21124250.

[15] A. R. Al Tahtawi, "Kalman Filter Algorithm Design for HC-SR04 Ultrasonic Sensor Data Acquisition System," International Journal of Information Technology & Electrical Engineering (IJITEE), 2022.

[16] J. Ho Chang, J. T. Yen và K. K. Shung, "High-Speed Digital Scan Converter for High-Frequency Ultrasound Sector Scanners," Ultrasonics, vol. 48, no. 5, pp. 444–452, Sep. 2008, , doi: 10.1016/j.ultras.2008.03.001.

[17] A. P. Berkhoff, H. J. Huisman, J. M. Thijssen, E. M. G. P. Jacobs, R. J. F. Homan, "Fast Scan Conversion Algorithms for Displaying Ultrasound Sector Images," Ultrasonic Imaging, vol. 16, no. 2, pp. 87–108, 1994, doi: 10.1177/016173469401600203.

[18] A. Priyanka, "A Survey On Super-Resolution Image Reconstruction Techniques," IJERT, vol. 7, no. III, Mar. 2014.

[19] L. P. Yaroslavsky, "Non-uniform sampling, image recovery from sparse data," arXiv:0808.3728, 2008.

[20] R. C. Gonzalez, R. E. Woods, and S. L. Eddins, Digital Image Processing Using MATLAB, 3rd ed., McGraw-Hill, 2020.